Earth Syst. Dynam. Discuss., 3, 1347–1389, 2012
www.earth-syst-dynam-discuss.net/3/1347/2012/
doi:10.5194/esdd-3-1347-2012

Earth System Dynamics Discussions

Dynamical and biogeochemical control on the decadal variability of ocean carbon fluxes

R. Séférian[1,2], L. Bopp[2], D. Swingedouw[2], and J. Servonnat[2]

[1]Centre National de Recherche de Météo-France, CNRM-GAME – URA1357, 42 Avenue Gaspard Coriolis, 31100 Toulouse, France
[2]Laboratoire du Climat et de l'Environnement, LSCE – UMR8212, L'Orme des Merisiers Bât. 712, 91191 Gif sur Yvette, France

Received: 26 November 2012 – Accepted: 18 December 2012 – Published: 21 December 2012

Correspondence to: R. Séférian (roland.seferian@lsce.ipsl.fr)

Published by Copernicus Publications on behalf of the European Geosciences Union.

Abstract

Several recent observation-based studies suggest that ocean anthropogenic carbon uptake has slowed down due to the impact of anthropogenic forced climate change. However, it remains unclear if detected changes over the recent time period can really be attributed to anthropogenic climate change or to natural climate variability (internal plus naturally forced variability). One large uncertainty arises from the lack of knowledge on ocean carbon flux natural variability at the decadal time scales. To gain more insights into decadal time scales, we have examined the internal variability of ocean carbon fluxes in a 1000-yr long preindustrial simulation performed with the Earth System Model IPSL-CM5A-LR. Our analysis shows that ocean carbon fluxes exhibit low-frequency oscillations that emerge from their year-to-year variability in the North Atlantic, the North Pacific, and the Southern Ocean. In our model, a 20-yr mode of variability in the North Atlantic air-sea carbon flux is driven by sea surface temperature variability and accounts for ~ 40 % of the interannual regional variance. The North Pacific and the Southern Ocean carbon fluxes are also characterized by decadal to multi-decadal modes of variability (10 to 50 yr) that account for 30–40 % of the interannual regional variance. But these modes are driven by the vertical supply of dissolved inorganic carbon through the variability of Ekman-induced upwelling and deep-mixing events. Differences in drivers of regional modes of variability stem from the coupling between ocean dynamics variability and the ocean carbon distribution, which is set by large-scale secular ocean circulation.

1 Introduction

In recent years, several observation-based and model-based studies have suggested that ocean anthropogenic carbon uptake has slowed down due to the impact of anthropogenic forced climate change in various ocean regions (e.g. Corbière et al., 2007; Le Quéré et al., 2007). However, the fact that these changes in ocean carbon fluxes are

ESDD
3, 1347–1389, 2012

caused by anthropogenic forced climate change within the last decades is still debated (e.g. Ullman et al., 2009; McKinley et al., 2011).

Among these regions potentially impacted by anthropogenic forced climate change, the North Atlantic has been extensively studied over the three last decades (Watson et al., 2011; Schuster et al., 2009; Brown et al., 2010; Metzl et al., 2010; Corbière et al., 2007; McKinley and Follows, 2004; McKinley et al., 2011). Debate prominently arises from disagreement between causes of trends in the North Atlantic carbon sink estimated from data or numerical model output. On the basis of in situ observations, several authors (i.e. Corbière et al., 2007; Watson et al., 2011; Brown et al., 2010; Metzl et al., 2010) have reported a more rapid growth in surface ocean pCO_2 than in atmospheric pCO_2, which translates into a decline of the net ocean carbon uptake over the last decade. Possible mechanisms driving this decline are associated to climate-induced modifications of both oceanic and atmospheric dynamics, e.g. rising sea-surface temperature (Corbière et al., 2007), increasing ocean stratification (Schuster et al., 2009) or changes in horizontal oceanic currents owing to a shift in the North Atlantic Oscillation (Thomas et al., 2007; Schuster et al., 2009). However, model reanalysis studies, based on GFDL, CCSM and MIT ocean general circulation reanalyses, have demonstrated that the weakening of the North Atlantic carbon sink over the last three decades (i.e. 1970s to 2000s) cannot be really attributed to anthropogenic climate change but rather to the natural variability of the ocean carbon sink driven by the North Atlantic Oscillation (McKinley et al., 2011; Thomas et al., 2008; Löptien and Eden, 2010) as a part of the Northern Annular Mode (NAM).

Similarly to the North Atlantic, many aspects of the Southern Ocean dynamics and carbon cycle have exhibited trends over the last decades. Model simulations and inversions of atmospheric data have suggested that the southward shift of westerlies concomitantly with their strengthening had dampened the Southern Ocean carbon sink (e.g. Le Quéré et al., 2007; Lovenduski and Ito, 2009). Such a response on ocean carbon fluxes has been highlighted by Lovenduski et al. (2008) on shorter time scales. In this study, authors demonstrated that the southward shift of westerlies associated

ESDD
3, 1347–1389, 2012

with the positive trend in the Southern Annular Mode (SAM) could drive a weakening of the Southern Ocean carbon sink because of changes in water mass overturning. However, it seems that such a response of both water mass overturning and ocean carbon sink may be overstated at the decadal time scale since no changes in Southern Ocean circulation have been detected from observations, while these data detect coherent warming and freshening trends in subsurface waters (Boening et al., 2008).

From these previous studies, it remains thus unclear if detected changes in ocean carbon sink within the last decades can be attributed to anthropogenic climate change or to natural climate variability that is a combination of an internal variability and a naturally forced variability (related to volcanoes and solar forcings). One large uncertainty arises from the lack of knowledge on ocean carbon flux variability at decadal time scales (Bates, 2007; Takahashi, 2009).

So far, these time scales has been an active fields of research in the ocean dynamics community (e.g. Latif et al., 2006, and references therein). Studies generally agree to the fact that sea-surface temperature and other ocean variables exhibit low-frequency modes of variability within mid and high latitude oceans (e.g. Latif et al., 2006; Zwiers, 1996; Boer, 2000, 2004). It is thus likely that the modes of variability of the ocean carbon fluxes could be inherited from low-frequency modes of variability like the Atlantic Multi-decadal Oscillation (AMO; e.g. Bates, 2012; McKinley and Follows, 2004; McKinley et al., 2011), or the Pacific Decadal Oscillation (PDO; e.g., Valsala et al., 2012; Takahashi et al., 2006) in a similar way as their interannual variability is mainly associated with the tropical Pacific ocean variability caused by El Niño and La Niña (e.g. Chavez et al., 1999; Wang and Moore, 2012; McKinley and Follows, 2004).

However, studying low-frequency variations in ocean carbon fluxes within these oceanic regions is not straightforward. The major limitation comes from the temporal coverage of the observations or model reanalysis. A good illustration of this limitation is to consider the North Atlantic sector that is one of the few places where large datasets (e.g. Gruber et al., 2002; Bakker et al., 2012) are available and where ocean reanalysis are consistent over the 30 to 50 last years to investigate multi-year variations in ocean

ESDD
3, 1347–1389, 2012

carbon fluxes (Ullman et al., 2009; Löptien and Eden, 2010; Thomas et al., 2008). Despite this large amount of information, an optimal spatial and temporal coverage of 30 to 50 yr provided by model reanalyses only allows studying 3 to 5 independent decades. Such limitation is thus even stronger for in situ observations. Observations are either combined and interpolated into large ocean regions in order to ensure a significant time sampling (McKinley et al., 2011), or considered as individual long-term stations (e.g. Gruber et al., 2002; Bates, 2007; Bates et al., 2012) that may be poorly representative of the basin-scale dynamics (McKinley and Follows, 2004).

In this context, long model simulations (> 500 yr) are the only mean to circumvent spatiotemporal sampling issues and have been demonstrated to be the minimum amount of data to assess significantly variability at decadal time-scales (e.g. Boer, 2004). The usefulness of long model simulations for studying temporal variations of land and ocean carbon fluxes was first illustrated in Doney et al. (2006). Based on a 1000-yr fully coupled climate-carbon cycle simulation, the authors provide a good overview of the natural variability of the global carbon cycle in CCSM-1.4. However, in this study, both decadal and oceanic aspects receive less attention than the interannual variability of the terrestrial carbon cycle.

Here, as a first step to assess the internal decadal variability of the ocean carbon fluxes, we used an extended 1000-yr long preindustrial simulation performed with the Earth System Model IPSL-CM5A-LR. Using output of this model simulation, we performed several statistical time-series analyses to (i) track the low-frequency modes variability, (ii) locate the oceanic regions that contribute the most to these modes and (iii) identify the main drivers of the ocean carbon fluxes variability at decadal time scales.

ESDD
3, 1347–1389, 2012

2 Methodology

2.1 Model description and pre-industrial simulation

This study exploits model output of IPSL-CM5A-LR (Dufresne et al., 2012), which contributes to the ongoing Coupled Model Intercomparison Project (CMIP5). IPSL-CM5A-LR combines the major components of the climate system: the atmosphere and land models are the atmospheric general circulation model LMDZ5A (Hourdin et al., 2012) and the land-surface model ORCHIDEE (Krinner et al., 2005). The atmospheric and land components use the same regular horizontal grid with 96×95 points, representing a resolution of $3.75^{\circ} \times 1.875^{\circ}$, while the atmosphere has 39 levels on the vertical. The oceanic component is NEMOv3.2 (Madec, 2008). It offers a horizontal resolution of 2° refined to 0.5° in the tropics and 31 vertical levels. NEMOv3.2 includes the sea ice model LIM2 (Fichefet and Maqueda, 1997), and the marine biogeochemistry model PISCES (Aumont and Bopp, 2006). PISCES simulates the biogeochemical cycles of carbon, oxygen and nutrients using 24 state variables. Macronutrients (nitrate and ammonium, phosphate, and silicate) and the micronutrient iron limit phytoplankton growth and thus improve the representation of their dynamics (Aumont et al., 2003; Aumont and Bopp, 2006). Inorganic carbon pools are dissolved inorganic carbon, alkalinity and calcite. Total alkalinity includes contributions from carbonate, bicarbonate, borate, hydrogen, and hydroxide ions (practical alkalinity). For dissolved CO_2 and O_2, air-sea exchange follows the quadratic wind-speed formulation (Wanninkhof, 1992).

The core of this study is an extended preindustrial simulation of 1000 yr, in which the initial state of marine carbon cycle comes from a 3000 yr offline spinup plus 300 yr of online adjustment, while the dynamical components of IPSL-CM5A-LR have been spun-up for 600 yr (Dufresne et al., 2012). Spin-up strategy and model-data skill-assessment of IPSL-CM5A-LR's marine biogeochemistry modern-state are presented and discussed in Séférian et al. (2012a).

ESDD
3, 1347–1389, 2012

2.2 Analytical methodology

The goals and methodology of this study are twofold. First, we aim at tracking and quantifying low-frequency oscillations of ocean carbon fluxes (here, decadal to multi-decadal internal variability). For that purpose, we employ several statistical time-series analyses like the continuous wavelet transform (Torrence, 1998), the spectral density or the principal component analysis (PCA; Von Storch and Zwiers, 2002).

Secondly we decipher which physical or biogeochemical drivers (here, alkalinity, dissolved inorganic carbon, salinity and temperature) control the various modes of variability of ocean carbon fluxes. We employ a decomposition of sea-water pCO_2 (driving the ocean carbon fluxes) based on Takahashi et al. (1993) assuming that pCO_2 is a function of Alkalinity (Alk), dissolved inorganic carbon (DIC), salinity (S) and temperature (T): $pCO_2 = f$ (Alk, DIC, T, S). The variance of the function of several random variables is given by expanding the function $f(X_1, X_2, X_3, ..., X_n)$ (here pCO_2) in Taylor series around the mean values of X (here, considered as the 1000-yr yearly-averaged climatology of Alk, DIC, S and T):

$$\mathrm{Var}\left(f\left(X_1, X_2, X_3, ..., X_n\right)\right) \approx \sum_{i=1}^{n} \left(\frac{\partial f}{\partial X_i}\right)^2 \sigma_{X_i}^2 + \sum_{i=1}^{n} \sum_{j \neq i}^{n} \frac{\partial f}{\partial X_i} \frac{\partial f}{\partial X_j} \mathrm{Cov}\left(X_i, X_j\right) \quad (1)$$

where $\sigma_{X_i}^2$ is the variance of the random variable X_i and $\mathrm{Cov}(X_i, X_j)$ is the covariance between the random variables X_i and X_j.

Based on this variance decomposition, we have conducted several offline computations of monthly-averaged sea-water pCO_2 and ocean carbon fluxes in which only one ocean carbon flux driver is allowed to vary in time while the others are fixed to their 1000-yr yearly-averaged climatology (Table 1). Online and offline computations of monthly-averaged sea-water pCO_2 and ocean carbon fluxes shows small differences in global average long-term mean and compares well in term of variability ($R \sim 0.96$).

Consequently, we assume that our variance decomposition strategy allows us to single out the variance contribution of Alk for pCO_2-Alk or fCO_2-Alk, DIC for pCO_2-DIC

ESDD
3, 1347–1389, 2012

or fCO_2-DIC and so on. A similar approach was used in previous studies (e.g. Ullman et al., 2009; McKinley and Follows, 2004).

As described in Boer (2000, 2004), we have removed linear drifts of ocean carbon fluxes and carbon-related fields since variables drifts matter for assessing low-frequency modes of variability. Yet, in our case drifts in sea-water pCO_2 and ocean carbon fluxes are small compared to the interannual or low-frequency oscillations: for global ocean carbon fluxes it represents about −0.03 Pg C over 100 yr in the first century of the 1000-yr simulation and only −0.01 Pg C over 100 yr in the last century of the 1000-yr simulation.

3 The preindustrial global ocean carbon fluxes

Hereafter, we present how the simulated carbon fluxes over the 1000 yr of preindustrial simulations compare to those estimated from inverse modeling by Mikaloff Fletcher et al. (2007), which constitute the only observation-based (even indirectly) product available for pre-industrial carbon fluxes. On Fig. 1a, the North Atlantic high latitude carbon sink amounts to about $-40\,g\,C\,m^{-2}\,yr^{-1}$ in average while the polar Southern Ocean is a source of about $20\,g\,C\,m^{-2}\,yr^{-1}$ in average. Regionally, the simulated oceanic sinks and sources of carbon agree with those estimated by inverse modeling with a global root-mean square error of about $0.06\,Pg\,C\,yr^{-1}$ (Fig. 1b). Only in the high latitude North West Pacific and the low latitude North Atlantic, ocean carbon fluxes differ in sign from those estimated by inverse modeling. In the southern sub-polar regions, the model biases can be explained by a shift of outgasing structures probably associated with the equator shift of main wind stress structures (Marti et al., 2009): compared to the inverse modeling-based estimates, our model simulates a stronger outgasing of carbon in the southern sub-polar Atlantic than in the southern sub-polar Pacific.

Now if we consider the time-variability over 1000 yr of the global ocean carbon flux in the preindustrial simulation, we can track low-frequency oscillations from its year-to-year variability (Fig. 2a). The 10-yr and 20-yr time-filtered variances amount

ESDD
3, 1347–1389, 2012

respectively to 0.08 and 0.05 Pg C yr^{-1} representing 56 and 37 % of the interannual variance (0.14 Pg C yr^{-1}).

The imprint of low-frequency modes of variability on the global carbon flux can be diagnosed from the autocorrelation function (ACF) of the global ocean carbon flux (Fig. 2b). The shape of the ACF does not correspond to a first order autoregressive process (AR1), but rather to a third order autoregressive process (AR3) according to the Yule-Walker estimation (Von Storch and Zwiers, 2002). The fact that the ACF of the global ocean carbon flux cannot be mimicked by an AR1 indicates that long-term memory processes likely drive ocean carbon fluxes. This implies that the ocean carbon flux behaves as other oceanic variables, like sea-surface temperature or sea-surface salinity (Frankignoul, 1985), but its low-frequency variability has a strong imprint over several years.

Low-frequency modes of the global ocean carbon flux variability range within a time-window of about 128 to 200 yr (centennial mode) and 18 to 50 yr (decadal mode) as shown on the wavelet time-frequency diagram (Fig. 1c and d). In comparison to the centennial mode, the decadal mode is not continuously detected. Nevertheless, the wavelet power spectrum within the decadal time-window is significantly stronger than a red noise wavelet spectrum (at 95 % in red dots, at 90 % in blue dots, Fig. 1d). The fact that the decadal mode appears sporadically over the time scales underlines the complexity of studying a globally integrated quantity, because such a behavior can be explained by a combination of several regional modes of variability either in phase or out of phase. As a consequence, in the next section, analyses will be conducted regionally.

4 Tracking the decadal mode of variability of the ocean carbon fluxes

Modes of variability of one variable are an expression of its variance at several time scales. Here, the way we apprehend these different modes of variability, in a first approach, is to look at the variance of the time-filtered carbon fluxes in several oceanic

ESDD
3, 1347–1389, 2012

regions, which correspond to those defined and used in Mikaloff Fletcher et al. (2007). The time filtering consists in a running mean of the regional carbon fluxes at 5, 10 and 20 yr (Fig. 3a). In high latitude oceans, the 1-, 5- and 10-yr variances are stronger compared to those found in mid and low-latitudes regions (i.e. $\sim 0.01\,\mathrm{Pg\,C\,yr^{-1}}$). Yet, it is striking to see how the Southern Ocean variances (i.e. for all time filtering) dominate those of the other oceanic regions with a standard deviation of about $0.1\,\mathrm{Pg\,C\,yr^{-1}}$. Such differences between the Southern Ocean and other oceanic regions are evidently fueled by differences in surface areas, much larger in the Southern Hemisphere regions than in the northern ones. As explained in Mikaloff Fletcher et al. (2007), region boundaries have been estimated using in situ measurements of ΔpCO_2 (Takahashi et al., 2002) and a general ocean circulation model, and have been designed consistently with TRANSCOM regions (Gurney et al., 2002). That is, each region differs greatly in surface area compared to each other. Therefore, surface area weighing allows comparing the different regions independently of their design (Fig. 3b). Yet, variability of surface area weighted carbon fluxes is still much stronger in mid and high latitude oceans than in the tropical ones.

In order to assess the relative importance of low-frequency modes of variability comparatively to interannual variability, we have employed a signal-to-noise ratio, the diagnosed potential predictability (DPP; Boer, 2004; Boer and Lambert, 2008; Persechino et al., 2012):

$$\mathrm{DPP} = \frac{\sigma_M^2 - \frac{1}{M}\sigma^2}{\sigma^2} \tag{2}$$

where σ^2 is the ocean carbon flux 1-yr variance and σ_M^2 ($M = 5$, 10 and 20 yr) is the variance of the time-filtered ocean carbon flux.

The DPP metric (Fig. 3c) indicates that the 5-yr and the 10-yr time-filtered variances of ocean carbon fluxes within the North Atlantic, the North Pacific and the Southern Ocean amounts for more than 30 % of the 1-yr variance. The Southern Ocean is the only oceanic region where multi-decadal variability of ocean carbon fluxes (here

ESDD
3, 1347–1389, 2012

represented by the 20-yr time-filtered variance) reaches up to 40 % of the 1-yr variance. These results are consistent with previous studies showing that low-frequency variability of various climate variables is mainly located in the high latitude oceans (Boer, 2000, 2004; Persechino et al., 2012; Mauget et al., 2011).

In particular, the three oceanic regions are characterized by well understood modes of variability in ocean dynamical fields: the AMO for the North Atlantic (Kerr, 2000; Enfield et al., 2001), the PDO for the North Pacific (Mantua and Hare, 2002) and the signature of the Southern Annular Mode on the Southern Ocean (Thompson and Wallace, 2000; Thompson et al., 2000). These various modes of variability have been suggested to have an influence on the variability of ocean carbon fields (Bates, 2012; McKinley and Follows, 2004; McKinley et al., 2011; Valsala et al., 2012; Takahashi et al., 2006; Lenton and Matear, 2007; Lovenduski et al., 2008). However, the fact that the signal-to-noise ratio of ocean carbon fluxes are comparable with those of other climate fields at regional scale with the same model (e.g. sea-surface temperature, sea-surface salinity; Persechino et al., 2012) does not mean that the modes of variability or even the drivers are the same.

To address this issue, we have computed empirical orthogonal functions (EOFs) of ocean carbon fluxes for the North Atlantic (10°–80° N), North Pacific (10° N–70° N) and the Southern Ocean (< 50° S). We have selected the five leading principal components (PCs), which explain together a minimum of 80 % of the regional carbon flux total variance. The ratio between regional and global interannual variances explained by the leading EOFs amounts to 12, 20 and 26 % in the North Atlantic, the North Pacific, and the Southern Ocean, respectively. As shown on Fig. 4, the spectral density of the five leading PCs of the regional carbon fluxes contains strong signals at decadal to multi-decadal time scales and displays large differences compared to a theoretical red-noise spectrum (AR1). The energy contained in the first mode of variability is always significantly stronger than the secondary modes except for the Southern Ocean for which the second mode of variability is stronger than the first mode at 5–10 yr.

ESDD
3, 1347–1389, 2012

Figure 4a shows a strong 20-yr mode of variability in the North Atlantic carbon flux, which is also found in several PCs (i.e. 1st, 3rd and 5th). The leading PC that accounts for 54 % of the total variance is the most energetic mode of variability. Compared to the leading PC, the second and the third PCs only account for 12 and 9 % of the total variance. The leading mode of the North Atlantic carbon flux variability has an amplitude of about 0.008 Pg C yr^{-1} that has been estimated from the standard deviation of the leading CP × EOF. Escudier et al. (2012) have found a similar signature of a 20-yr mode in the North Atlantic in the same model and have explained this mode of variability by the interplay between SSS, SST and sea-ice cover with implications on mixed-layer depth anomalies in the sub-polar gyre and Nordic Seas.

In comparison to the North Atlantic, the various modes of variability found in the North Pacific and the Southern Ocean carbon fluxes differ at the decadal time scales. In the North Pacific, modes of variability range between 10 to 30 yr (Fig. 4b). The three leading PCs, which account for 76 % of the total variance, have a large part of their energy in a time-window of 10 to 30 yr. In this time-window, the leading PC explains 44 % of the total variance and presents modes of variability at 10 and 30 yr. The standard deviation of the leading CP × EOF associated with the multi-decadal modes of variability contribute to ∼ 0.03 Pg C yr^{-1} to the North Pacific carbon flux variability.

In the Southern Ocean, the leading PC (34 % of the total variance) sheds light on a prominent mode of variability at 50 yr, while a decadal mode of variability is found in the second PC that amounts to 28 % of the total variance (Fig. 4c). Among these different modes, variability is stronger for the first 50-yr mode than for the others. This mode has a magnitude of about 0.05 Pg C yr^{-1}. Figure 4c shows also a centennial mode of variability that appears in all of the PCs. However, this mode of variability cannot be thoroughly studied with a 1000-yr time-series. Similar results are found for regional-averaged surface pCO_2 (not shown).

ESDD
3, 1347–1389, 2012

5 Identifying drivers of low-frequency variability of ocean carbon fluxes

A further step is to identify drivers and examine their respective role in explaining the low-frequency variability of ocean carbon fluxes described in the previous sections. To find out what drivers contribute the most to the low-frequency variability of the ocean carbon fluxes, we use the variance decomposition detailed in Eq. (1) and Table 1. With this variance decomposition, we have conducted PCA analysis to identify correspondence in patterns and time variability between the fully-driven ocean carbon fluxes (fCO_2) and fluxes driven only by Alk, DIC, S and T, named respectively fCO_2-Alk, fCO_2-DIC, fCO_2-SSS and fCO_2-SST. Figures 5 to 7 show the leading EOF for the North Atlantic, North Pacific and the Southern Ocean carbon fluxes, while lagged correlation between the leading PC of ocean carbon fluxes and dynamical drivers, i.e. sea-surface temperature, mixed-layer depth (MLD) and sea level pressure (SLP) are presented in Fig. 8. These dynamical drivers have been chosen since they are proxies of climate modes of variability (i.e. the AMO, the PDO, the NAM and the SAM).

The various climate indexes have been estimated from the leading EOF and PC of SST for the AMO and the PDO, and those of SLP for the NAM and the SAM. Their definition differ from their canonical definition, especially for the AMO and PDO index, which are usually estimated from the 10-yr running mean of detrended SST north of the equator over the Atlantic (Enfield et al., 2001; Kerr, 2000) and Pacific (Mantua and Hare, 2002), respectively. Here, our definition of AMO and PDO index on the basis of PCA analysis show a significant correlation (>0.42) with their canonical index estimated from the same 1000-yr long preindustrial simulation. That is, our definition of AMO and PDO mode of variability can be understood as a good approximation of their canonical definition.

In the North Atlantic, fCO_2 exhibits a horseshoe pattern, in addition to a dipole structure located close to the ocean convection sites of the Labrador and the Irminger Seas. Such features are also found in the leading EOFs of fCO_2-DIC and fCO_2-SST (Fig. 5c and e). The leading EOF of the fCO_2-SST exhibits an AMO-like pattern that is also

ESDD
3, 1347–1389, 2012

highlighted in Ullman et al. (2009) using the MIT OGCM reanalysis over 1992–2006. In our model, the leading fCO_2-SST mode of variability displays a good match with the AMO-like pattern (Table 2). The respective correlations between PCs indicate a better match between time variability of fCO_2 and that of fCO_2-SST ($R \sim 0.6$) than that of fCO_2-DIC ($R \sim 0.3$). Regarding fCO_2-Alk and fCO_2-SSS, the leading EOF spatial patterns and the respective PCs are poorly correlated with the fCO_2 (Fig. 5b and d).

Regarding variations between SST, MLD and SLP with those of fCO_2, lagged correlations indicate that the leading mode of fCO_2 variability is strongly in phase with that of SST (Fig. 8). Significant correlations are also found between the leading PC of SLP and that of fCO_2 but can be understood as a feedback of the dynamical coupling occurring between the atmosphere and the ocean in the North Atlantic sector. Indeed, recent studies based on model simulations (Gastineau and Frankignoul, 2012) or observation-derived climate index (Rossi et al., 2011; D'Aleo and Easterbrook, 2011; McCarthy et al., 2012) have argued that oceanic influence through SST variations lead the Northern Hemisphere climate (e.g. SLP) by a few years explaining the slightly lagged inverse relationship found between the NAM/NAO and the AMO climate index. This seems to be the case in our model since cross-correlation between the leading PC of SLP and that of SST (not shown) displays strong correlation at lag −1/0 of about 0.64. Correlation between the leading PCs of fCO_2 and MLD seems to indicate that fCO_2 variations lead those of MLD. Such a result may be explained by the large regional boundaries that include several site of deep convection that are either in phase or out of phase. Nonetheless, the presence of 10-yr-lagged oscillations in correlation coefficients between MLD and fCO_2 (also in SST) can be explained by the 20-yr cycle occurring in the North Atlantic sector in this model (Escudier et al., 2012).

In the North Pacific, the leading EOF presents a strong positive pattern in the northern part of the domain (Fig. 6a), which is located at the same place as the strong North Pacific carbon outgasing (Fig. 1a). Such a pattern appears for fCO_2-DIC, but not for fCO_2-Alk, fCO_2-SSS and fCO_2-SST (Fig. 6). The leading EOF of the fCO_2-SST exhibits a PDO-like pattern and presents good agreement with the PDO diagnosed from

ESDD
3, 1347–1389, 2012

the leading SST EOF (Table 2). This implies that SSTs imprint a low-frequency signature on the ocean carbon fluxes (Valsala et al., 2012), but are not the major driver of the ocean carbon flux variability in the North Pacific. The temporal correlations of the respective driver-related PCs with that of fCO_2 demonstrate that variability driven by DIC mainly controls this mode of variability ($R > 0.9$).

Lagged correlations (Fig. 8) between leading PCs of fCO_2 and dynamical drivers point toward a significant role of the mixed-layer depth ($R \sim 0.4$ at lag 0) and the SLP ($R \sim 0.1$ at lag 0). This supports the fact that both Ekman-induced upwelling and winter deep-mixing events bring DIC-rich deep waters at surface contributing to the fCO_2 variability. The strong lagged correlation at 2 yr found in SST and SLP leading PCs are related to the mid-latitudes wind regimes over the North Pacific and can be, at worst, considered as an artifact of the large regional boundaries we have chosen to define the North Pacific (10° N–70° N). They do not appear if one focuses above 40° N, while the strong correlation between fCO_2 and MLD and SLP are reinforced ($R > 0.5$ at lag 0).

The Southern Ocean differs from other oceanic regions due to its zonal structure and its ocean dynamical features like the Antarctic Circumpolar Current, the westerlies forcings and the near-shelf dense water mass formation. Such dynamical features influence the ocean carbon cycle and are mirrored on the leading EOF (Fig. 7a). A linear decomposition of drivers shows that leading EOFs of the different driver-related fCO_2 present a good agreement with that of fCO_2 ($R > 0.4$). This strong spatial correlation is mainly associated with the strong spot of variability close to the Antarctic shelf. Yet, the temporal variability of the fCO_2-DIC strongly agrees with that of fCO_2 ($R > 0.9$).

To better understand Southern Ocean modes of variability, we have considered two sub-regions: one close to the Antarctic shelf and the sea-ice border (< 65° S) and the second that extends from 65° S to 45° S, strongly influenced by the westerlies. In the wind-driven region, the leading EOF of fCO_2-DIC strongly matches with the fCO_2 one ($R \sim 0.8$). This result agrees with several studies, which have demonstrated that westerlies influence the vertical supply of DIC through the outcrop of deep water masses (Lenton and Matear, 2007; Lovenduski et al., 2008). In this sub-region, the prominent

ESDD
3, 1347–1389, 2012

mode of variability is at 10 yr, and appears consistently within the second mode of variability of Southern Ocean carbon fluxes (Fig. 4c).

In the sea ice-driven region, PCA analysis shows instead that fCO_2 appears to be driven rather by SSS than by DIC with a spatial correlation of about 0.7 and 0.5 respectively. Yet, temporal correlations indicate a better correspondence with DIC-driven variability ($R \sim 0.87$) than the SSS-driven variability ($R \sim 0.2$).

Similarly to the North Pacific, it seems that the MLD and the SLP variations drive the variability of the fCO_2 in the Southern Ocean, not the SST. Two different processes take place: on the one hand, close to the sea-ice shelf, the deep-convection events occurring during winter mix subsurface DIC-rich waters with surface waters. This process is linked to sea ice variability that also drives a fraction of the SSS spatiotemporal variability. On the other hand, in the open sea, the wind forcing influences the subduction of intermediate and mode waters around Antarctica (Sallée et al., 2012) and Ekman-induced upwelling of deep-core waters. At decadal time scales, it is likely that the SAM oscillations could influence the Deacon cell through the Ekman-induced transport bringing in turn DIC-rich deep waters (Table 2). This may explain why we find a lag at 5–8 yr for the cross-correlation between SLP and fCO_2 leading PCs. In the whole Southern Ocean region ($< 50^{\circ}$ S), this mode linking SAM and ocean carbon fluxes, appears only as a second mode with a correlation of 0.7 at lag 0 indicating that this mechanism is of second order compared to the deep-mixing events linked to ocean-sea ice interactions.

In order to show how variability in ocean dynamics can interact with water mass properties in terms of dissolved carbon, we show the long-term mean and variance concentration of DIC, Alk and Alk-DIC at the maximum (winter) of the mixed-layer depth (Fig. 9). Alk-DIC serves as a good approximation for the carbonate ion concentration (Sarmiento and Gruber, 2006). This is a proxy for the buffer capacity of seawater and hence the chemical capacity for the ocean to take up atmospheric CO_2. Figure 9c indicates that the sub-surface water masses are rich in DIC content with an Alk-DIC concentration close to 0. It appears thus clearly that, of the three different oceanic

ESDD
3, 1347–1389, 2012

regions, the chemical properties of the North Pacific and the Southern Ocean subsurface water masses differ greatly from those of the North Atlantic.

In regions of water mass formation (i.e. North Atlantic), the water mass content in DIC is set by air-sea interaction and biology, and is hence sensitive to both variations in atmospheric forcings and variations in surface ocean properties (i.e. SST). In regions of water mass outcrops and transformations (i.e. North Pacific and Southern Ocean), water mass content in DIC is instead enriched by remineralization processes occurring below the surface. Consequently, response of ocean carbon fluxes driven at first order by the difference in partial pressure of CO_2 between the atmosphere and the surface waters (which have been replenished in DIC due to DIC-rich deep water mass upwelling) overcomes the variability inherited from ocean thermodynamical variables like the SST and SSS. Such processes are highlighted in Fig. 10 showing respectively long-term mean state and variance profile of pCO_2, Alk-pCO_2, DIC-pCO_2, SSS-pCO_2 and SST-pCO_2. Long-term mean vertical profiles of pCO_2-Alk, pCO_2-DIC, pCO_2-SSS and pCO_2-SST exhibit large differences in pCO_2 at 500 m between the North Atlantic, the North Pacific and the Southern Ocean (Fig. 10a–c). The pCO_2 long-term mean profile in the North Atlantic displays an important vertical gradient in the first 100 m and a well-mixed profile below (Fig. 10a). This is not the case for the North Pacific and the Southern Ocean pCO_2 profile, which exhibit a strong gradient from surface to 500 m (Fig. 10b and c). Within these two regions, the variability of pCO_2 at 500 m (here, the standard deviation) is 5- to 6-fold stronger than the North Atlantic one.

Figure 10j–l present results of a multiple linear regression on the basis of Eq. (1). Statistical t-test on each parameter slope (here, Alk, DIC, S and T) can be considered as an attribution test. That is, there is attribution of the variability driven by a given parameter to the pCO_2 variability if the slope is close to 1. There is no attribution if the slope is negative or if the confidence interval of the slope includes 0. Consequently, our attribution test demonstrates that the variations (Fig. 10d–f) of pCO_2 at depth are mostly explained by variations in temperature in the North Atlantic with an attribution factor close to 1, while North Pacific and Southern Ocean pCO_2 variations at depth are

ESDD
3, 1347–1389, 2012

set by variations in DIC with an attribution factor close to 1. Others variables like S and Alk have a poor contribution to the pCO_2 variability.

6 Conclusions

In this study, using a 1000-yr long preindustrial simulation performed with the Earth System Model IPSL-CM5A-LR, we have examined the decadal internal variability of ocean carbon fluxes as a part of their natural variability. Our results suggest that the low-frequency variability of ocean carbon fluxes (and sea-water pCO_2) emerges from year-to-year variability in all high latitude oceans. Low-frequency modes of variability display substantial differences in their periods of oscillation between the various oceanic basins. The North Atlantic carbon flux exhibits a strong 20-yr mode of oscillation while the North Pacific and the Southern Ocean carbon fluxes present several modes extending over a decade or more. The prominent modes of variability are a 10-yr and a 30-yr mode in the North Pacific and a 50-yr mode in the Southern Ocean. These modes of variability of carbon fluxes in the North Pacific and in the Southern Ocean are mostly driven by the variability of the dissolved inorganic carbon of surface waters. The latter is controlled by the vertical supply of dissolved inorganic carbon of subsurface waters, through the dynamical influence of wind forcings or deep-mixing events, which controls the shape and the timing of the carbon flux variability within these regions. In the North Atlantic, the ocean carbon flux is primarily driven by the variability of sea surface temperature. This contrast in dynamical and biogeochemical drivers of ocean carbon flux variations between the three oceanic regions is set in part by the large-scale circulation of water masses and their biogeochemical properties. That is, in regions of dense water mass outcrops and transformations, variations in vertical supply of dissolved inorganic carbon (owing to Ekman-induced upwelling or deep-mixing events) are of larger amplitude than the variations inherited from thermodynamical properties of surface waters (owing to ocean-atmosphere or ocean-sea ice interactions). This is not the case in regions of dense water mass formation.

ESDD
3, 1347–1389, 2012

The fact that low-frequency variations in ocean carbon fluxes are simulated in our model within high latitude oceans is consistent with previous studies conducted on dynamical fields like sea surface temperature, surface air temperature or precipitation (e.g. Boer, 2004, 2000). Of particular interest, a similar study with the same model (i.e. IPSL-CM5A-LR) by Persechino et al. (2012) demonstrates that decadal variations of sea surface temperature amount for 20 % (with a maximum of 50 %) of their interannual variations within the North Atlantic sector. Comparatively, ocean carbon fluxes exhibit low-frequency variations much stronger (∼ 30–40 %) than those of sea surface temperature. Such differences between low-frequency variations of ocean carbon fluxes and other dynamical fields are even stronger in the Southern Ocean, where Boer (2004) shows that multi-model zonal average variations of surface air temperature at decadal time scales only accounts for 10 % of the interannual variability. In our case, decadal variations of ocean carbon fluxes within Subpolar and Polar Regions of the Antarctic sector amounts to up to 50 %. Such features can be explained by the statistical properties of ocean carbon fluxes, which cannot be approximated with a first-order autoregressive process (like other dynamical variables mentioned above) indicating that long-term memory processes likely drive ocean carbon fluxes (and potentially others biogeochemical fluxes like the carbon export, the primary productivity and the remineralization).

Also related to long-memory processes, all of these oceanic regions exhibit multi-centennial modes of variability (> 150 yr) that cannot be assessed with a 1000-yr preindustrial simulation. Similar multi-centennial modes of variability have also been revealed in sea-surface temperature, sea-surface salinity, sea-ice volume and Atlantic meridional overturning for the GFDL-CM2.1 climate model (Delworth and Zeng, 2012). Interestingly this study has hypothesized that these modes are controlled by interactions between ocean and sea-ice dynamics. It is thus likely that such interactions could impact air-sea carbon fluxes.

At decadal time scales, processes related to these low-frequency modes of variability agree with process-based studies (Ullman et al., 2009; Corbière et al., 2007; Löptien

ESDD
3, 1347–1389, 2012

and Eden, 2010; Thomas et al., 2008; Metzl et al., 2010; Lovenduski et al., 2008; Takahashi et al., 2006), which suggest that variations in air-sea fluxes (or sea-water partial pressure) of carbon are driven either by the sea surface temperature or by the vertical supply of dissolved inorganic carbon. However, our results seem to indicate that vertical supply of dissolved organic carbon related to the atmospheric modes of variability are of major importance in the North Pacific and the Southern Ocean, not directly in the North Atlantic. Indeed, in our model, atmospheric modes of variability like the North Atlantic Oscillation weakly impact the ocean carbon fluxes (or very locally) as mentioned in Keller et al. (2012), while they can be projected on ocean-atmosphere coupled modes like the Atlantic Multi-decadal Oscillation. Nevertheless, we shall keep in mind that these findings are subject to criticism because they are related to the fact that we use only one Earth System Model. Consequently, we can wonder: (1) how modes of variability of a given Earth System Model compare to each other? (2) Is there any consistency between their drivers? Therefore, studies like the one conducted by Keller et al. (2012) are of great interest in order to understand how a given Earth System Model behaves in a multi-model perspective.

Yet, even in a multi-model perspective such as CMIP5, one of the major uncertainties in the quantification of the internal variability of ocean carbon fluxes (as others variables) would be related to the horizontal resolution of ocean model ($> 1^{\circ}$ in most of the CMIP5 models). Recent literature (e.g. Penduff et al., 2011, 2010) highlights that meso-scale activity in eddying-region like the Southern Ocean strongly enhances interannual variability of ocean variables – such as ocean turbulence. The impact of meso-scale activity could likely amplify the interannual variability of the ocean carbon fluxes. Since the variability of the ocean carbon fluxes is influenced by the long-term mean state of ocean carbon-related fields, this variability could be affected by the response of westerlies-induced transport to the model resolution (e.g. Farneti et al., 2010; Hofmann and Morales Maqueda, 2011) and hence model biases (Swart and Fyfe, 2011).

Notwithstanding the limitations of the model, our findings provide a first step to better understand the role of the internal variability (as a part of the natural variability)

ESDD
3, 1347–1389, 2012

versus that of the anthropogenic forced variability on the ocean carbon fluxes. Our results demonstrate that care should be taken while analyzing short-term changes with delta or biases correction methods assuming that the long-term mean state does not affect the variability, while it does matter in some oceanic regions like the Southern Ocean and the North Pacific. This is not the case for long-term changes for which rising atmospheric CO_2 and climate change can impact ocean carbon fluxes much more strongly than their decadal variations (Matear and Lenton, 2008; Lenton and Matear, 2007; Séférian et al., 2012b; Roy et al., 2011).

Then, the issue of what observations may be most useful to constrain predictions of the ocean carbon fluxes within decades has received much less attention than the issue of disentangling the decadal natural variability from its secular anthropogenic trend (McKinley et al., 2011). Both issues are important, but the observational needs are different. To assess and quantify the observational need in the view of studying the natural variability of ocean carbon fluxes, similar studies to that of Lenton et al. (2009) could be a possible alternative.

Acknowledgements. We sincerely thank Marina Levy, Corinne Le Quéré, Marion Gehlen and Mehera Kidston for their usefull comments on that paper. This work was supported by GENCI (Grand Equipement National de Calcul Intensif) at CCRT (Centre de Calcul Recherche et Technologie), allocation 016178 and through EU FP7 project CARBOCHANGE "Changes in carbon uptake and emissions by oceans in a changing climate" which received funding from the European Community's Seventh Framework Programme under grant agreement no. 264879.

References

Aumont, O. and Bopp, L.: Globalizing results from ocean in situ iron fertilization studies, Global Biogeochem. Cy., 20, GB2017, doi:10.1029/2005GB002591, 2006. 1352

Aumont, O., Maier-Reimer, E., Blain, S., and Monfray, P.: An ecosystem model of the global ocean including Fe, Si, P colimitations, Global Biogeochem. Cy., 17, 1060, doi:10.1029/2001GB001745, 2003. 1352

ESDD

3, 1347–1389, 2012

Bakker, D. C. E., Pfeil, B., Olsen, A., Sabine, C. L., Metzl, N., Hankin, S., Koyuk, H., Kozyr, A., Malczyk, J., Manke, A., and Telszewski, M.: Global data products help assess changes to ocean carbon sink, Eos Trans. AGU, 93, doi:10.1029/2012EO120001, 2012. 1350

Bates, N. R.: Interannual variability of the oceanic CO_2 sink in the subtropical gyre of the North Atlantic Ocean over the last 2 decades, J. Geophys. Res., 112, C09013, doi:10.1029/2006JC003759, 2007. 1350, 1351

Bates, N. R.: Multi-decadal uptake of carbon dioxide into subtropical mode water of the North Atlantic Ocean, Biogeosciences, 9, 2649–2659, doi:10.5194/bg-9-2649-2012, 2012. 1350, 1357

Bates, N. R., Best, M. H. P., Neely, K., Garley, R., Dickson, A. G., and Johnson, R. J.: Detecting anthropogenic carbon dioxide uptake and ocean acidification in the North Atlantic Ocean, Biogeosciences, 9, 2509–2522, doi:10.5194/bg-9-2509-2012, 2012. 1351

Boening, C. W., Dispert, A., Visbeck, M., Rintoul, S., and Schwarzkopf, F. U.: The response of the Antarctic Circumpolar Current to recent climate change, Nat. Geosci., 1, 864–869, 2008. 1350

Boer, G. J.: A study of atmosphere-ocean predictability on long time scales, Clim. Dynam., 16, 469–477, doi:10.1007/s003820050340, 2000. 1350, 1354, 1357, 1365

Boer, G. J.: Long time-scale potential predictability in an ensemble of coupled climate models, Clim. Dynam., 23, 29–44, doi:10.1007/s00382-004-0419-8, 2004. 1350, 1351, 1354, 1356, 1357, 1365

Boer, G. J. and Lambert, S. J.: Multi-model decadal potential predictability of precipitation and temperature, Geophys. Res. Lett., 35, L05706, doi:10.1029/2008GL033234, 2008. 1356

Bretherton, C. S., Widmann, M., Dymnikov, V. P., Wallace, J. M., and Bladé, I.: The effective number of spatial degrees of freedom of a time-varying field, J. Climate, 12, 1990–2009, 1999. 1387

Brown, P. J., Bakker, D. C. E., Schuster, U., and Watson, A. J.: Anthropogenic carbon accumulation in the subtropical North Atlantic, J. Geophys. Res., 115, C04016, doi:10.1029/2008JC005043, 2010. 1349

Chavez, F. P., Strutton, P. G., Friederich, G. E., Feely, R., Feldman, G. C., Foley, D. G., and McPhaden, M. J.: Biological and Chemical Response of the Equatorial Pacific Ocean to the 1997–98 El Niño, Science, 286, 2126–2131, doi:10.1126/science.286.5447.2126, 1999. 1350

ESDD
3, 1347–1389, 2012

Corbière, A., Metzl, N., Reverdin, G., Brunet, C., and Takahashi, T.: Interannual and decadal variability of the oceanic carbon sink in the North Atlantic subpolar gyre, Tellus B, 59, 168–178, doi:10.1111/j.1600-0889.2006.00232.x, 2007. 1348, 1349, 1365

D'Aleo, J. and Easterbrook, D.: Chapter 5 – Relationship of Multidecadal Global Temperatures to Multidecadal Oceanic Oscillations, in: Evidence-Based Climate Science, Elsevier, Boston, 161–184, doi:10.1016/B978-0-12-385956-3.10005-1, 2011. 1360

Delworth, T. L. and Zeng, F.: Multicentennial variability of the Atlantic meridional overturning circulation and its climatic influence in a 4000 year simulation of the GFDL CM2.1 climate model, Geophys. Res. Lett., 39, L13702, doi:10.1029/2012GL052107, 2012. 1365

Doney, S. C., Lindsay, K., Fung, I., and John, J.: Natural Variability in a Stable, 1000-Yr Global Coupled Climate–Carbon Cycle Simulation, J. Climate, 19, 3033–3054, doi:10.1175/JCLI3783.1, 2006. 1351

Dufresne, J.-L., Foujouls, M.-A., Denvil, S., Caubel, A., Marti, O., Aumont, O., Balkansky, Y., Bekki, S., Bellenger, S., Benshila, R., Bony, S., Bopp, L., Braconnot, P., and Brockmann, P.: The IPSL-CM5A Earth System Model: general description and climate change projections, Clim. Dynam., submitted, 2012. 1352

Enfield, D. B., Mestas Nuñez, A. M., and Trimble, P. J.: The Atlantic Multidecadal Oscillation and its relation to rainfall and river flows in the continental U.S., Geophys. Res. Lett., 28, 2077–2080, doi:10.1029/2000GL012745, 2001. 1357, 1359

Escudier, R., Mignot, J., and Swingedouw, D.: A 20-year coupled ocean-sea ice-atmosphere variability mode in the North Atlantic in an AOGCM, Clim. Dynam., doi:10.1007/s00382-012-1402-4, in press, 2012. 1358, 1360

Farneti, R., Delworth, T. L., Rosati, A. J., Griffies, S. M., and Zeng, F.: The Role of Mesoscale Eddies in the Rectification of the Southern Ocean Response to Climate Change, J. Phys. Oceanogr., 40, 1539–1557, doi:10.1175/2010JPO4353.1, 2010. 1366

Fichefet, T. and Maqueda, M. A. M.: Sensitivity of a global sea ice model to the treatment of ice thermodynamics and dynamics, J. Geophys. Res., 102, 12609–12646, 1997. 1352

Frankignoul, C.: Sea surface temperature anomalies, planetary waves, and air-sea feedback in the middle latitudes, Rev. Geophys., 23, 357–390, doi:10.1029/RG023i004p00357, 1985. 1355

Gastineau, G. and Frankignoul, C.: Cold-season atmospheric response to the natural variability of the Atlantic meridional overturning circulation, Clim. Dynam., 39, 37–57, doi:10.1007/s00382-011-1109-y, 2012. 1360

ESDD
3, 1347–1389, 2012

Gruber, N., Keeling, C., and Bates, N.: Interannual variability in the North Atlantic Ocean carbon sink, Science, 298, 2374–2378, 2002. 1350, 1351

Gurney, K. R., Law, R. M., Denning, A. S., Rayner, P. J., Baker, D., Bousquet, P., Bruhwiler, L., Chen, Y.-H., Ciais, P., Fan, S., Fung, I. Y., Gloor, M., Heimann, M., Higuchi, K., John, J., Maki, T., Maksyutov, S., Masarie, K., Peylin, P., Prather, M., Pak, B. C., Randerson, J., Sarmiento, J., Taguchi, S., Takahashi, T., and Yuen, C.-W.: Towards robust regional estimates of CO_2 sources and sinks using atmospheric transport models, Nature, 415, 626–630, doi:10.1038/415626a, 2002. 1356

Hofmann, M. and Morales Maqueda, M. A.: The response of Southern Ocean eddies to increased midlatitude westerlies: A non-eddy resolving model study, Geophys. Res. Lett., 38, L03605, doi:10.1029/2010GL045972, 2011. 1366

Hourdin, F., Foujols, M.-A., Codron, F., Guemas, V., Dufresne, J.-L., Bony, S., Denvil, S., Guez, L., Lott, F., Ghattas, J., Braconnot, P., Marti, O., Meurdesoif, Y., and Bopp, L.: Impact of the LMDZ atmospheric grid configuration on the climate and sensitivity of the IPSL-CM5A coupled model, Clim. Dynam., doi:10.1007/s00382-012-1411-3, in press, 2012. 1352

Keller, K. M., Joos, F., Raible,, C. C., Cocco, V., Froelicher, T. L., Dunne, J. P., Gehlen, M., Roy, T., Bopp, L., Orr, J. C., Tjiputra, J., Heinze, C., Segschneider, J., and Metzl, N.: Variability of the Ocean Carbon Cycle in Response to the North Atlantic Oscillation, Tellus B, 64, 18738, doi:10.3402/tellusb.v64i0.18738, 2012. 1366

Kerr, R. A.: A North Atlantic Climate Pacemaker for the Centuries, Science, 288, 1984–1985, 2000. 1357, 1359

Krinner, G., Viovy, N., de Noblet-Ducoudré, N., Ogée, J., Polcher, J., Friedlingstein, P., Ciais, P., Sitch, S., and Prentice, I.: A dynamic global vegetation model for studies of the coupled atmosphere-biosphere system, Global Biogeochem. Cy., 19, 1–33, 2005. 1352

Latif, M., Collins, M., Pohlmann, H., and Keenlyside, N.: A review of predictability studies of Atlantic sector climate on decadal time scales, J. Climate, 19, 5971–5987, doi:10.1175/JCLI3945.1, 2006. 1350

Le Quéré, C., Roedenbeck, C., Buitenhuis, E. T., Conway, T. J., Langenfelds, R., Gomez, A., Labuschagne, C., Ramonet, M., Nakazawa, T., Metzl, N., Gillett, N., and Heimann, M.: Saturation of the Southern Ocean CO_2 sink due to recent climate change, Science, 316, 1735–1738, doi:10.1126/science.1136188, 2007. 1348, 1349

ESDD
3, 1347–1389, 2012

Lenton, A. and Matear, R. J.: Role of the Southern Annular Mode (SAM) in Southern Ocean CO_2 uptake, Global Biogeochem. Cy., 21, GB2016, doi:10.1029/2006GB002714, 2007. 1357, 1361, 1367

Lenton, A., Bopp, L., and Matear, R. J.: Strategies for high-latitude northern hemisphere CO_2 sampling now and in the future, Deep-Sea Res. Pt. II, 56, 523–532, doi:10.1016/j.dsr2.2008.12.008, 2009. 1367

Löptien, U. and Eden, C.: Multidecadal CO_2 uptake variability of the North Atlantic, J. Geophys. Res., 115, D12113, doi:10.1029/2009JD012431, 2010. 1349, 1351, 1365

Lovenduski, N. S. and Ito, T.: The future evolution of the Southern Ocean CO_2 sink, J. Mar. Res., 67, 597–617, doi:10.1357/002224009791218832, 2009. 1349

Lovenduski, N. S., Gruber, N., and Doney, S. C.: Toward a mechanistic understanding of the decadal trends in the Southern Ocean carbon sink, Global Biogeochem. Cy., 22, GB3016, doi:10.1029/2007GB003139, 2008. 1349, 1357, 1361, 1366

Madec, G.: NEMO ocean engine, france edn., Institut Pierre-Simon Laplace (IPSL), institut pierre-simon laplace (ipsl), France, 2008. 1352

Mantua, N. and Hare, S.: The Pacific Decadal Oscillation, J. Oceanogr., 58, 35–44, doi:10.1023/A:1015820616384, 2002. 1357, 1359

Marti, O., Braconnot, P., Dufresne, J.-L., Bellier, J., Benshila, R., Bony, S., Brockmann, P., Cadule, P., Caubel, A., Codron, F., Noblet, N., Denvil, S., Fairhead, L., Fichefet, T., Foujols, M. A., Friedlingstein, P., Goosse, H., Grandpeix, J. Y., Guilyardi, E., Hourdin, F., Idelkadi, A., Kageyama, M., Krinner, G., Lévy, C., Madec, G., Mignot, J., Musat, I., Swingedouw, D., and Talandier, C.: Key features of the IPSL ocean atmosphere model and its sensitivity to atmospheric resolution, Clim. Dynam., 34, 1–26, doi:10.1007/s00382-009-0640-6, 2009. 1354

Matear, R. J. and Lenton, A.: Impact of Historical Climate Change on the Southern Ocean Carbon Cycle, J. Climate, 21, 5820–5834, doi:10.1175/2008JCLI2194.1, 2008. 1367

Mauget, S. A., Cordero, E. C., and Brown, P. T.: Evaluating Modeled Intra- to Multidecadal Climate Variability Using Running Mann-Whitney Z Statistics, J. Climate, 25, 110824105314 003, doi:10.1175/JCLI-D-11-00211.1, 2011. 1357

McCarthy, G. D., King, B. A., Cipollini, P., MCDonagh, E., Blundell, J. R., and Biastoch, A.: On the sub-decadal variability of South Atlantic Antarctic Intermediate Water, Geophys. Res. Lett., 39, L10605, doi:10.1029/2012GL051270, 2012. 1360

ESDD
3, 1347–1389, 2012

McKinley, G. A., Follows, M. J., and Marshall, J.: Mechanisms of air-sea CO2 flux variability in the equatorial Pacific and the North Atlantic, Global Biogeochem. Cy., 18, GB2011, doi:10.1029/2003GB002179, 2004. 1349, 1350, 1351, 1354, 1357

McKinley, G. A., Fay, A. R., Takahashi, T., and Metzl, N.: Convergence of atmospheric and North Atlantic carbon dioxide trends on multidecadal timescales, Nat. Geosci., 4, 1–5, doi:10.1038/ngeo1193, 2011. 1349, 1350, 1351, 1357, 1367

Metzl, N., Corbière, A., Reverdin, G., Lenton, A., Takahashi, T., Olsen, A., Johannessen, T., Pierrot, D., Wanninkhof, R., Ólafsdóttir, S. R., Olafsson, J., and Ramonet, M.: Recent acceleration of the sea surface fCO_2 growth rate in the North Atlantic subpolar gyre (1993–2008) revealed by winter observations, Global Biogeochem. Cy., 24, GB4004, doi:10.1029/2009GB003658, 2010. 1349, 1366

Mikaloff Fletcher, S. E., Gruber, N., Jacobson, A. R., Gloor, M., Doney, S. C., Dutkiewicz, S., Gerber, M., Follows, M., Joos, F., Lindsay, K., Menemenlis, D., Mouchet, A., Müller, S. A., and Sarmiento, J. L.: Inverse estimates of the oceanic sources and sinks of natural CO_2 and the implied oceanic carbon transport, Global Biogeochem. Cy., 21, GB1010, doi:10.1029/2006GB002751, 2007. 1354, 1356, 1378

Penduff, T., Juza, M., Brodeau, L., Smith, G. C., Barnier, B., Molines, J.-M., Treguier, A.-M., and Madec, G.: Impact of global ocean model resolution on sea-level variability with emphasis on interannual time scales, Ocean Sci., 6, 269–284, doi:10.5194/os-6-269-2010, 2010. 1366

Penduff, T., Juza, M., Barnier, B., Zika, J., Dewar, W. K., Treguier, A.-M., Molines, J.-M., and Audiffren, N.: Sea Level Expression of Intrinsic and Forced Ocean Variabilities at Interannual Time Scales, J. Climate, 24, 5652–5670, doi:10.1175/JCLI-D-11-00077.1, 2011. 1366

Persechino, A., Mignot, J., Swingedouw, D., Labetoulle, S., and Guilyardi, E.: Decadal predictability of the Atlantic meridional overturning circulation and climate in the IPSL-CM5A-LR model, Clim. Dynam., doi:10.1007/s00382-012-1466-1, in press, 2012. 1356, 1357, 1365

Rossi, A., Massei, N., and Laignel, B.: A synthesis of the time-scale variability of commonly used climate indices using continuous wavelet transform, Global Planet. Change, 78, 1–13, doi:10.1016/j.gloplacha.2011.04.008, 2011. 1360

Roy, T., Bopp, L., Gehlen, M., Schneider, B., Cadule, P., Frölicher, T. L., Segschneider, J., Tjiputra, J., Heinze, C., and Joos, F.: Regional Impacts of Climate Change and Atmospheric CO_2 on Future Ocean Carbon Uptake: A Multimodel Linear Feedback Analysis, J. Climate, 24, 2300–2318, doi:10.1175/2010JCLI3787.1, 2011. 1367

ESDD
3, 1347–1389, 2012

Sallée, J.-B., Matear, R. J., Rintoul, S. R., and Lenton, A.: Localized subduction of anthropogenic carbon dioxide in the Southern Hemisphere oceans, Nat. Geosci., 5, 579–584, doi:10.1038/ngeo1523, 2012. 1362

Sarmiento, J. L. and Gruber, N.: Ocean Biogeochemical Dynamics, Princeton University Press, 2006. 1362

Schuster, U., Watson, A. J., Bates, N. R., Corbiere, A., González-Dávila, M., Metzl, N., Pierrot, D., and Santana-Casiano, M.: Trends in North Atlantic sea-surface fCO_2 from 1990 to 2006, Deep-Sea Res. Pt. II, 56, 620–629, doi:10.1016/j.dsr2.2008.12.011, 2009. 1349

Séférian, Roland, Bopp, L., Gehlen, M., Orr, J., Ethé, C., Cadule, P., Aumont, O., Salas y Mélia, D., Voldoire, A., and Madec, G.: Skill assessment of three earth system models with common marine biogeochemistry, Clim. Dynam., doi:10.1007/s00382-012-1362-8, in press, 2012a. 1352

Séférian, R., Iudicone, D., Bopp, L., Roy, T., and Madec, G.: Water Mass Analysis of Effect of Climate Change on Air-Sea CO_2 Fluxes: The Southern Ocean, J. Climate, 25, 3894–3908, doi:10.1175/JCLI-D-11-00291.1, 2012b. 1367

Swart, N. C. and Fyfe, J. C.: Ocean carbon uptake and storage influenced by wind bias in global climate models, Nat. Clim. Change, 2, 47–52, doi:10.1038/nclimate1289, 2011. 1366

Takahashi, T.: Climatological mean and decadal change in surface ocean pCO_2, and net sea-air CO_2 flux over the global oceans, Deep Sea Res. Pt. II, 56, 554–577, doi:10.1016/j.dsr2.2008.12.009, 2009. 1350

Takahashi, T., Olafsson, J., Goddard, J. G., Chipman, D. W., and Sutherland, S. C.: Seasonal variation of CO_2 and nutrients in the high-latitude surface oceans: A comparative study, Global Biogeochem. Cy., 7, 843–878, doi:10.1029/93GB02263, 1993. 1353

Takahashi, T., Sutherland, S. C., Sweeney, C., Poisson, A., Metzl, N., Tilbrook, B., Bates, N., Wanninkhof, R., Feely, R. A., Sabine, C., Olafsson, J., and Nojiri, Y.: Global sea-air CO_2 flux based on climatological surface ocean pCO_2, and seasonal biological and temperature effects, Deep-Sea Res. Pt. II, 49, 1601–1622, doi:10.1016/S0967-0645(02)00003-6, 2002. 1356

Takahashi, T., Sutherland, S. C., Feely, R. A., and Wanninkhof, R.: Decadal change of the surface water pCO_2 in the North Pacific: A synthesis of 35 years of observations, J. Geophys. Res., 111, C07S05, doi:10.1029/2005JC003074, 2006. 1350, 1357, 1366

ESDD
3, 1347–1389, 2012

Thomas, H., Friederike Prowe, A. E., van Heuven, S., Bozec, Y., de Baar, H. J. W., Schiettecatte, L.-S., Suykens, K., Koné, M., Borges, A. V., Lima, I. D., and Doney, S. C.: Rapid decline of the CO_2 buffering capacity in the North Sea and implications for the North Atlantic Ocean, Global Biogeochem. Cy., 21, GB4001, doi:10.1029/2006GB002825, 2007. 1349

Thomas, H., Friederike Prowe, A. E., Lima, I. D., Doney, S. C., Wanninkhof, R., Greatbatch, R. J., Schuster, U., and Corbière, A.: Changes in the North Atlantic Oscillation influence CO_2 uptake in the North Atlantic over the past 2 decades, Global Biogeochem. Cy., 22, GB4027, doi:10.1029/2007GB003167, 2008. 1349, 1351, 1366

Thompson, D. W. J. and Wallace, J. M.: Annular modes in the extratropical circulation, Part I: month-to-month variability, J. Climate, 13, 1000–1016, 2000. 1357

Thompson, D. W. J., Wallace, J. M., and Hegerl, G. C.: Annular Modes in the Extratropical Circulation, Part II: Trends, J. Climate, 13, 1018–1036, 2000. 1357

Torrence, C. and Compo, G. P.: A Practical Guide to Wavelet Analysis, Bull. Amer. Meteor. Soc., 79, 61–78, doi:10.1175/1520-0477(1998)079<0061:APGTWA>2.0.CO;2, 1998. 1353

Ullman, D. J., McKinley, G. A., Bennington, V., and Dutkiewicz, S.: Trends in the North Atlantic carbon sink: 1992–2006, Global Biogeochem. Cy., 23, GB4011, doi:10.1029/2008GB003383, 2009. 1349, 1351, 1354, 1360, 1365

Valsala, V., Maksyutov, S., Telszewski, M., Nakaoka, S., Nojiri, Y., Ikeda, M., and Murtugudde, R.: Climate impacts on the structures of the North Pacific air-sea CO_2 flux variability, Biogeosciences, 9, 477–492, doi:10.5194/bg-9-477-2012, 2012. 1350, 1357, 1361

Von Storch, H. and Zwiers, F.: Statistical Analysis in Climate Research – Hans Von Storch, Francis W. Zwiers – Google Books, Cambridge University Press, 2002. 1353, 1355

Wang, S. and Moore, J. K.: Variability of primary production and air-sea CO_2 flux in the Southern Ocean, Global Biogeochem. Cy., 26, GB1008, doi:10.1029/2010GB003981, 2012. 1350

Wanninkhof, R.: A relationship between wind speed and gas exchange over the ocean, J. Geophys. Res., 97, 7373–7382, 1992. 1352

Watson, A. J., Metzl, N., and Schuster, U.: Monitoring and interpreting the ocean uptake of atmospheric CO_2, Philosophical Transactions of the Royal Society A: Mathematical, Phys. Eng. Sci., 369, 1997–2008, doi:10.1098/rsta.2011.0060, 2011. 1349

Zwiers, F.: Interannual variability and predictability in an ensemble of AMIP climate simulations conducted with the CCC GCM2, Clim. Dynam., 12, 825–847, 1996. 1350

ESDD
3, 1347–1389, 2012

Table 1. Description of the distinct ocean carbon fluxes (fCO_2) or oceanic partial pressure of carbon (pCO_2) driven by the variability of solely one drivers (i.e. T/SST, S/SSS, DIC or Alk) compared to the fully-driven ocean carbon fluxes.

	Alkalinity (Alk)	Dissolved Inorganic Carbon (DIC)	Salinity (S)	Temperature (T)
Fully-Driven	Interannual Variability	Interannual Variability	Interannual Variability	Interannual Variability
Alk-driven	Interannual Variability	1000-yr mean state	1000-yr mean state	1000-yr mean state
DIC-driven	1000-yr mean state	Interannual Variability	1000-yr mean state	1000-yr mean state
S-driven	1000-yr mean state	1000-yr mean state	Interannual Variability	1000-yr mean state
T-driven	1000-yr mean state	1000-yr mean state	1000-yr mean state	Interannual Variability

ESDD
3, 1347–1389, 2012

Table 2. Temporal correlation (R^2) at lag 0 between the Atlantic Multidecadal Oscillation (AMO), the Pacific Decadal Oscillation (PDO), the Northern Annular Mode (NAM) and the Southern Annular Mode (SAM) with the driver-related carbon fluxes (i.e. Alk-fCO_2, DIC-fCO_2, SSS-fCO_2, SST-fCO_2). t-test at 95 % of significance are mentioned in bold (following Bretherton et al., 1999). AMO and PDO index have been estimated from the leading PC of SST over the North Atlantic (10° N–80° N) and the North Pacific (10° N–70° N), respectively. NAM and SAM index have been computed from the leading PC of SLP over the North Atlantic (10° N–80° N) and the Southern ocean(< 50° S), respectively.

	Alk-fCO_2	DIC-fCO_2	SSS-fCO_2	SST-fCO_2
AMO	**0.79**	**0.68**	**0.77**	**0.95**
PDO	**0.42**	0.004	**0.73**	**0.95**
NAM	0.05	0.01	0.02	**0.17**
SAM	0.13	**0.30**	0.19	**0.59**

ESDD
3, 1347–1389, 2012

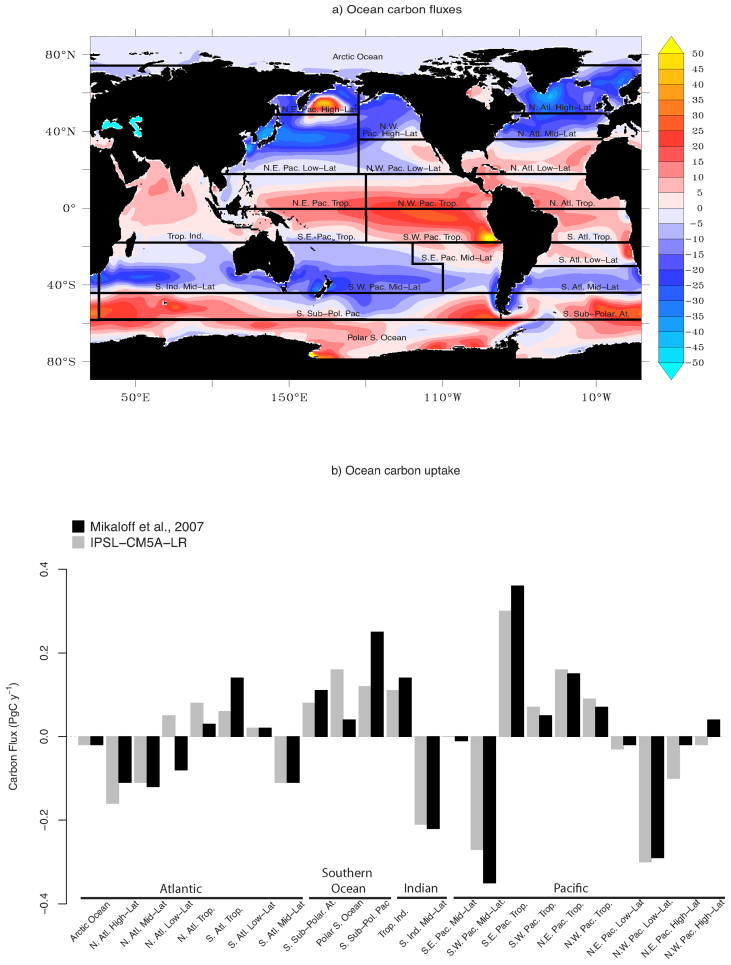

Fig. 1. Caption on next page.

ESDD
3, 1347–1389, 2012

Fig. 1. Long-term mean of **(a)** ocean carbon fluxes (in $g\,C\,m^{-2}\,yr^{-1}$) and **(b)** simulated regional carbon fluxes (in $Pg\,C\,yr^{-1}$) compared to inversion-based estimates published in Mikaloff Fletcher et al. (2007). Black and grey bars indicate model and inversion-based estimates respectively.

ESDD
3, 1347–1389, 2012

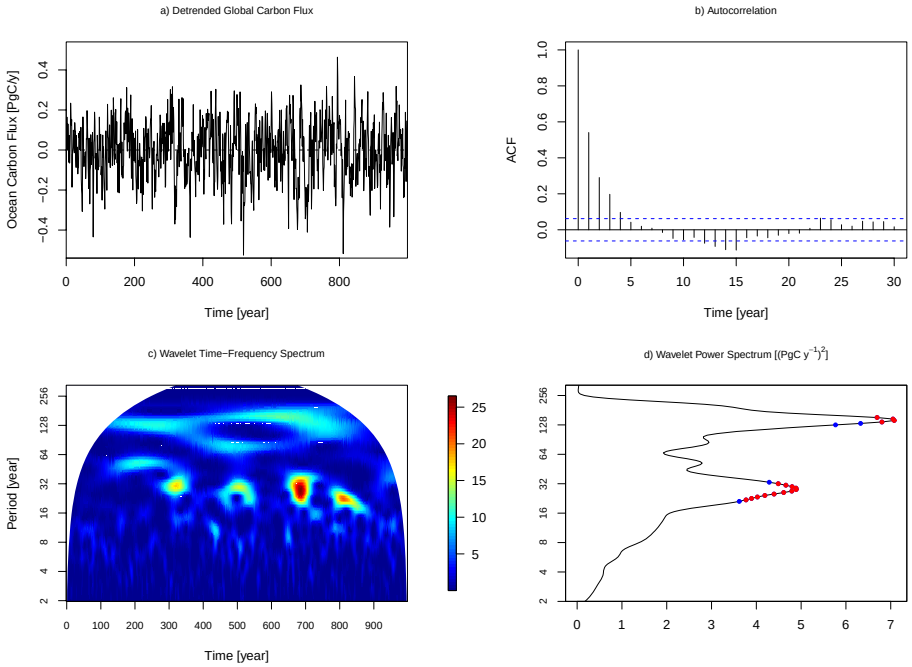

Fig. 2. Interannual time-series of the drift-corrected global ocean carbon flux (in $\mathrm{Pg\,C\,yr^{-1}}$) is represented in **(a)**. The autocorrelation function **(b)**, the wavelet time-frequency spectrum **(c)** and the averaged wavelet spectrum **(d)** describe the statistical properties of the drift-corrected global ocean carbon flux. A red noise hypothesis has been tested against the averaged wavelet spectrum. The significance of 95 % is mentioned with red points, while those of 90 % is mentioned in blue.

ESDD
3, 1347–1389, 2012

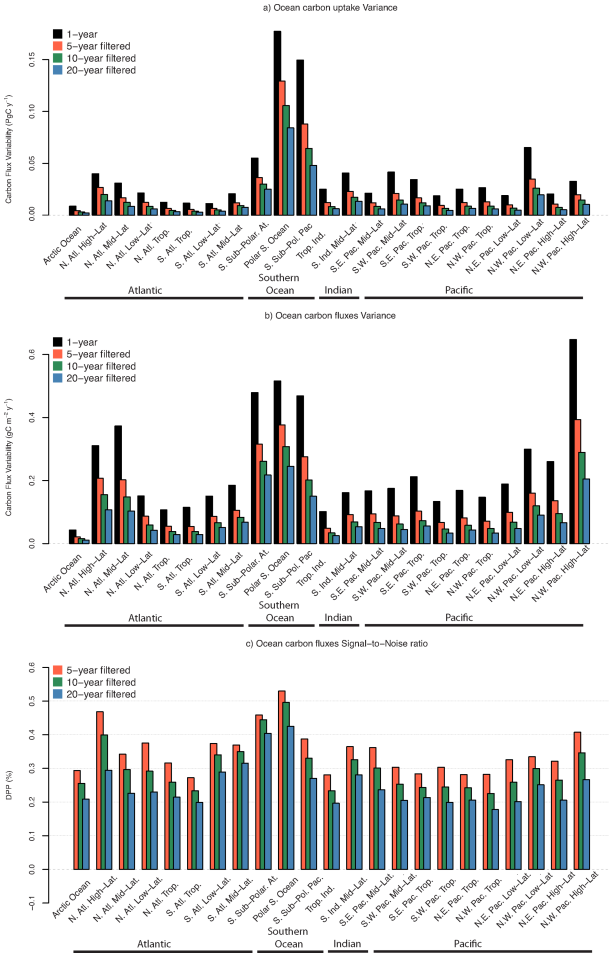

Fig. 3. Caption on next page.

ESDD
3, 1347–1389, 2012

Fig. 3. Regional variability of **(a)** the ocean carbon uptake (in $Pg\,C\,yr^{-1}$) and the area-weighted carbon fluxes (in $g\,C\,m^{-2}\,yr^{-1}$) at **(a)** 1-yr (interannual), 5-yr, 10-yr and 20-yr time-scales. The signal-to-noise ratio **(c)** of these different variances is estimated by DPP metric (Eq. 2) for the various oceanic regions.

ESDD
3, 1347–1389, 2012

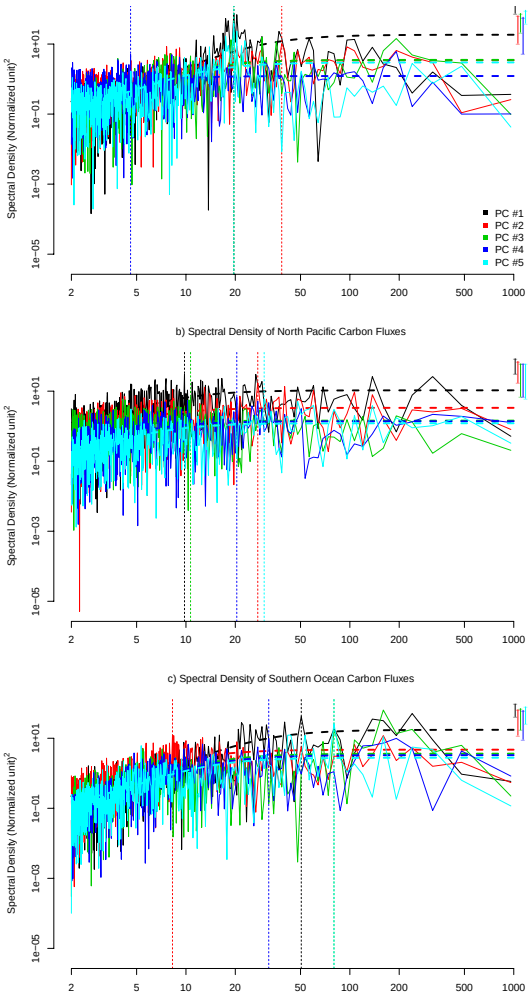

Fig. 4. Caption on next page.

ESDD
3, 1347–1389, 2012

Fig. 4. Scaled spectral density of the five leading principal components of ocean carbon fluxes for **(a)** the North Atlantic (10° N–80° N), **(b)** the North Pacific (10° N–70° N) and **(c)** the Southern ocean(< 50° S). Dashed lines represent fitted AR1 theoretical spectrum according to the Yule-Walker estimation, while the linear dashed lines indicate the maximum of spectral density for each principal components. Confidence intervals at 95 % of significance of the scaled spectral density maximum is indicated by vertical bars; they have been computed from a (scaled) χ^2 distribution.

ESDD
3, 1347–1389, 2012

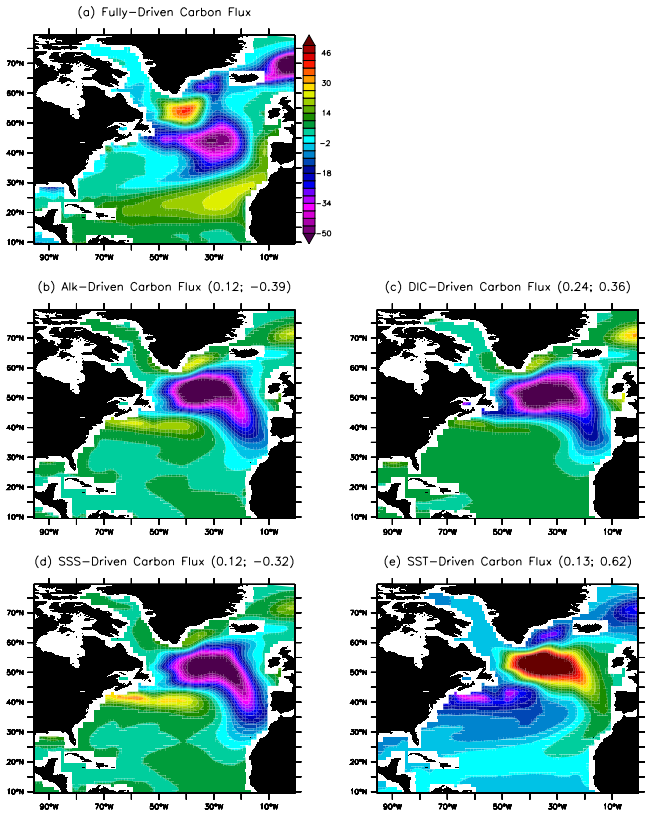

Fig. 5. Spatial pattern of the leading empirical orthogonal function (EOF, in normalized unit) of **(a)** the fully-driven carbon fluxes, and that of the Alk-driven **(b)**, DIC-driven **(c)**, SSS-driven **(d)** and SST-driven **(e)** ocean carbon fluxes in the North Atlantic. Spatial and temporal correlations between the fully-driven ocean carbon fluxes and each driver-related carbon fluxes are mentioned into brackets.

ESDD
3, 1347–1389, 2012

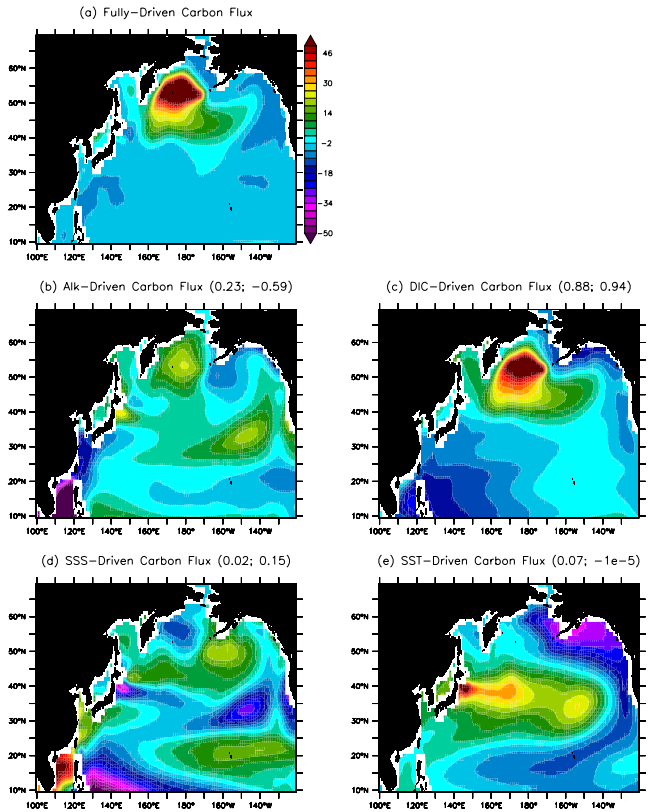

Fig. 6. Spatial pattern of the leading empirical orthogonal function (EOF, in normalized unit) of **(a)** the fully-driven carbon fluxes, and that of the Alk-driven **(b)**, DIC-driven **(c)**, SSS-driven **(d)** and SST-driven **(e)** ocean carbon fluxes in the North Pacific. Spatial and temporal correlations between each driver-related and the fully-driven ocean carbon fluxes are mentioned into brackets.

ESDD
3, 1347–1389, 2012

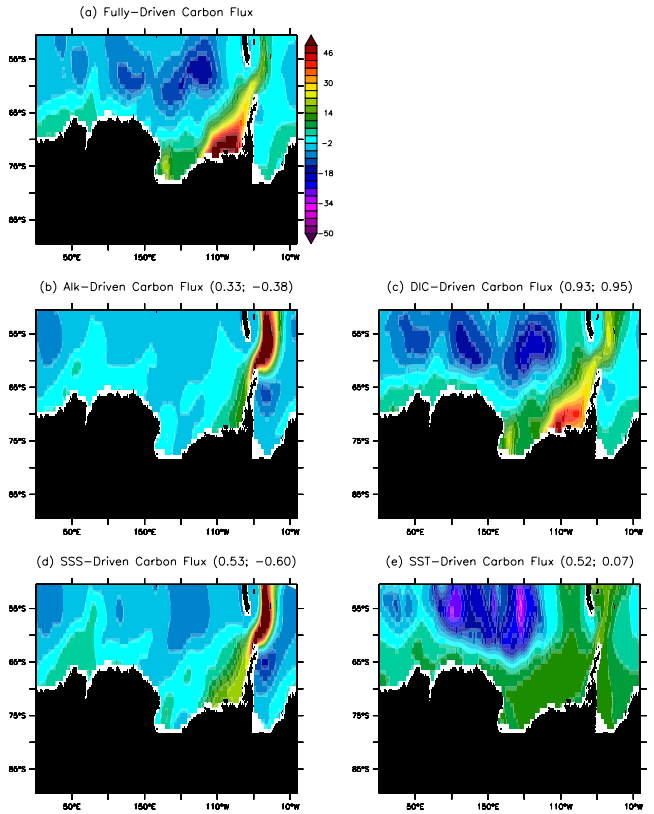

Fig. 7. Spatial pattern of the leading empirical orthogonal function (EOF, in normalized unit) of **(a)** the fully-driven carbon fluxes, and that of the Alk-driven **(b)**, DIC-driven **(c)**, SSS-driven **(d)** and SST-driven **(e)** ocean carbon fluxes in the Southern ocean. Spatial and temporal correlations between the fully-driven ocean carbon fluxes and each driver-related carbon fluxes are mentioned into brackets.

ESDD
3, 1347–1389, 2012

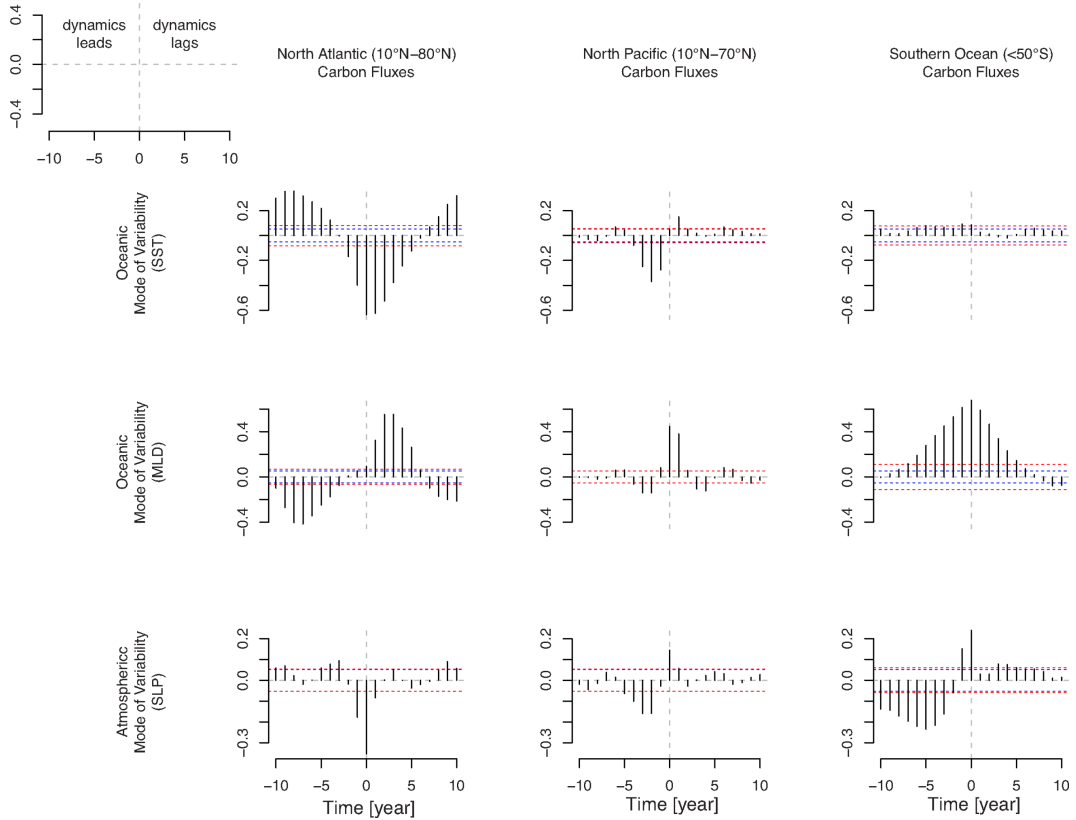

Fig. 8. Lagged correlation of leading principal compenents of ocean carbon fluxes and sea-surface temperature (SST), mixed-layer depth (MLD), sea-level pressure (SLP) in the North Atlantic, the North Pacific and the Southern Ocean carbon fluxes. t-test at 95 % of significance are mentioned with dashed blue lines and red lines (following Bretherton et al., 1999).

ESDD
3, 1347–1389, 2012

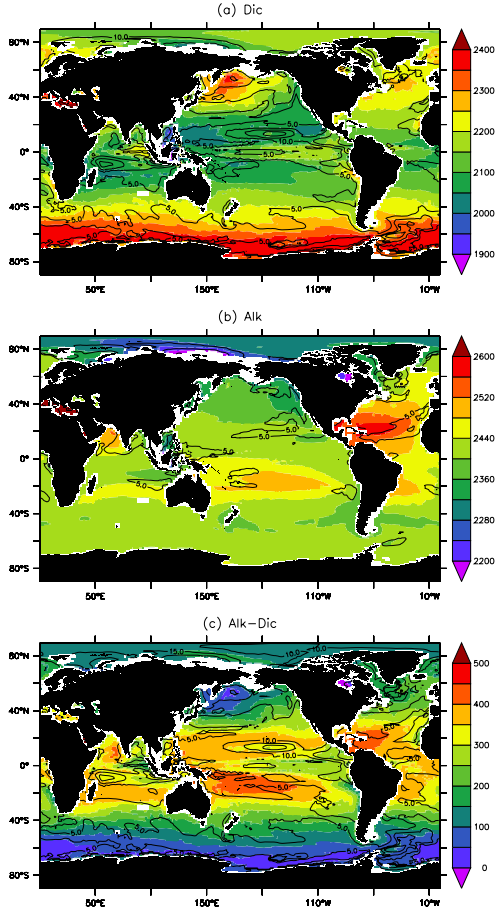

Fig. 9. Long-term mean of **(a)** DIC, **(b)** Alk and **(c)** Alk-DIC concentrations (in $\mu mol\,L^{-1}$) at maximum (winter) mixed-layer depth. Variability represented by the standard deviation of the concentrations of **(a)** DIC, **(b)** Alk and **(c)** Alk-DIC is countoured.

ESDD
3, 1347–1389, 2012

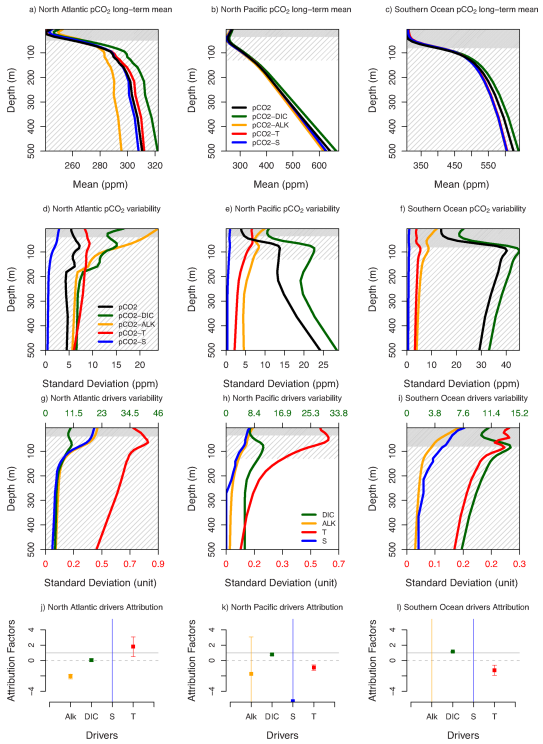

Fig. 10. Vertical profiles of the fully-driven, Alk-driven,DIC-driven, SSS-driven and SST-driven pCO_2. Panels **(a)**–**(c)** present long-term mean, **(d)**–**(f)** the variability of the fully-driven and driver-related pCO_2, while panels **(g)**–**(i)** concern the variance of the Alk, DIC, S and T. Panels **(j)**–**(l)** present attributing factor (coefficients of the multiple linear regression on the basis of Eq. 1) for the North Atlantic, the North Pacific and the Southern Ocean respectively. Confidence intervals have been computed from a t-test at 95 %. Attribution of a drivers variability to the pCO_2 variability requires an attribution factor close to 1 (horizontal grey line). Otherwise, there is no attribution for a given driver, if confidence interval includes 0 (horizontal dashed grey line).

ESDD
3, 1347–1389, 2012